Supplementary Materials

Tuning Correlations in an Oxide Mott System Using a Solid-State Field Effect Device

Lishai Shoham, Itai Silber, Gal Tuvia, Maria Baskin, Soo-Yoon Hwang, Si-Young Choi, Myung-Geun Han, Yimei Zhu, Eilam Yalon, Marcelo J. Rozenberg, Yoram Dagan, Felix Trier, and Lior Kornblum

1. Film characterization

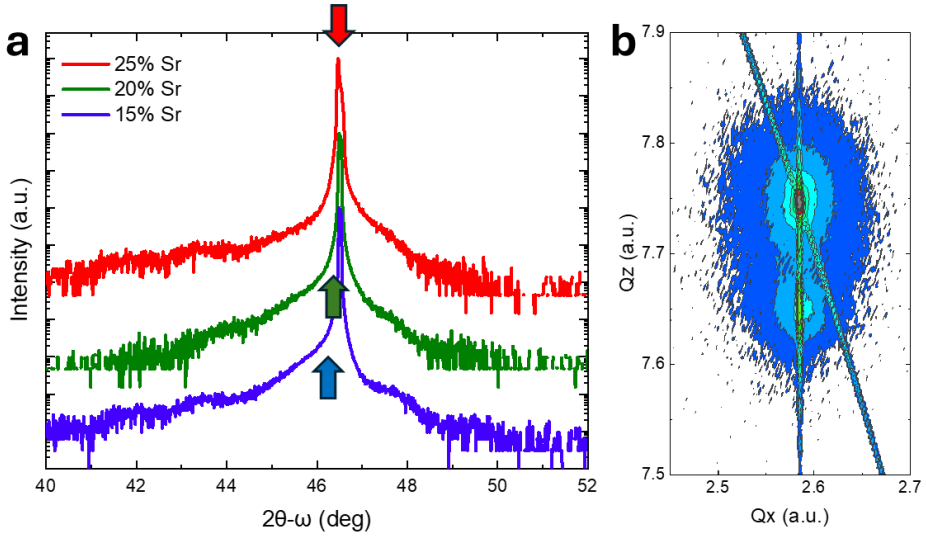

Figure S1. Structural analysis of the $La_{1-x}Sr_xVO_3$ (LSVO) films. (a) X-ray diffraction patterns around the cubic/pseudocubic (002) Bragg reflection of ~4 nm LSVO films grown on $SrTiO_3$ (STO) substrates. The arrows indicate the location of the film's (002) peak as simulated using the Global Fit software. The scans were taken prior to the Hall bar patterning, from the same samples that were later used for the electrical measurements in the main text. (b) A reciprocal space map (RSM) scan around the (013) Bragg reflection of the STO substrate with a comparable but thicker 27 nm $La_{0.75}Sr_{0.25}VO_3$ film, showing coherent growth. All measurements were taken using a Rigaku SmartLab with a two-bounce incident monochromator.

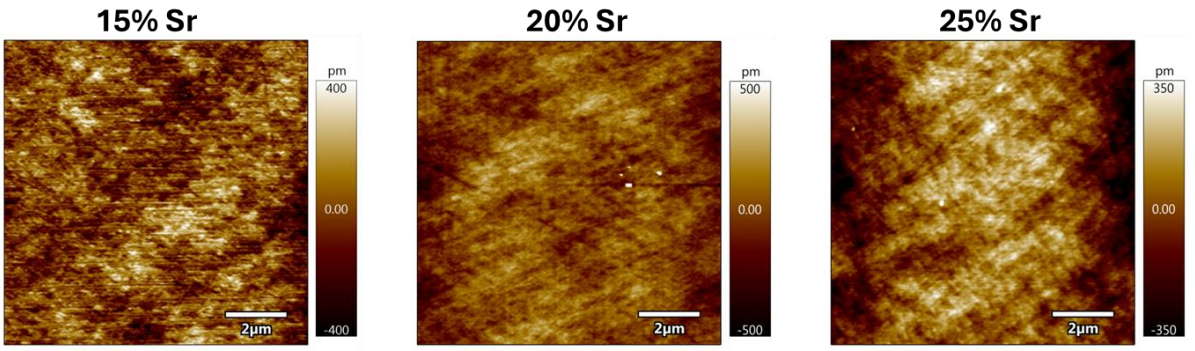

Figure S2. Surface morphology of the LSVO films prior to patterning illustrating a smooth surface (no substrate termination). The scans were acquired via an Asylum Research/Oxford Instruments Cypher ES Environmental atomic force microscope (AFM) operated in tapping mode.

2. Comparison of thick and thin films

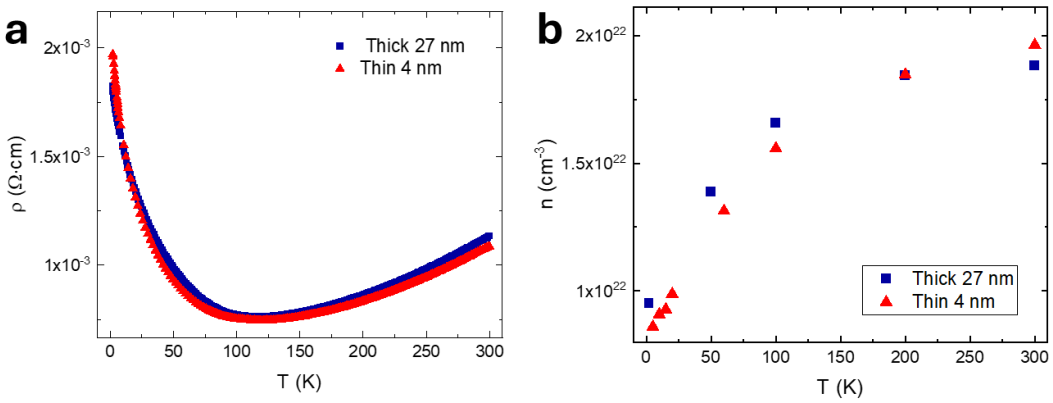

Figure S3. Magnetotransport comparison of $La_{0.75}Sr_{0.25}VO_3$ on STO substrate for Hall bar device (~4 nm) and a "thick" 27 nm film. (a) Temperature-dependent resistivity and (b) Temperature-dependent carrier density extracted from Hall measurements. For simplicity, we assume $n \approx n_H \approx (R_H e)^{-1}$ for a single-channel conduction (see discussion in the following section). The high resemblance of the results suggests a minor surface scattering in the Hall bar channel.

3. Mobility

Since the gate-induced charge variation of the LSVO Hall bar devices is negligible (see main text), we attribute the resistance response to the variation in mobility. Before attributing the mobility variation to changes in the electron correlations (manifest in the effective mass of the electrons, m*), we ruled out mobility degradation of the electrons under the gate electric field. Figure S4 presents the mobility of the LSVO devices at different temperatures, where the Hall response to the magnetic field was linear. The results illustrate that the mobility is relatively

constant for the measured temperature range, and more importantly, decreases with the increase of electron density. Based on Matthiessen's rule, we expect that the mobility degradation under gate electric field would be more significant for the device with a higher mobility. However, comparing for example the resistance response between 20 and 25% Sr concentration at 10K (Figure S6), we can see that the resistance response of the 20% is about an order of magnitude higher than the response of the 25% device, thus ruling out significant mobility degradation in the LSVO devices.

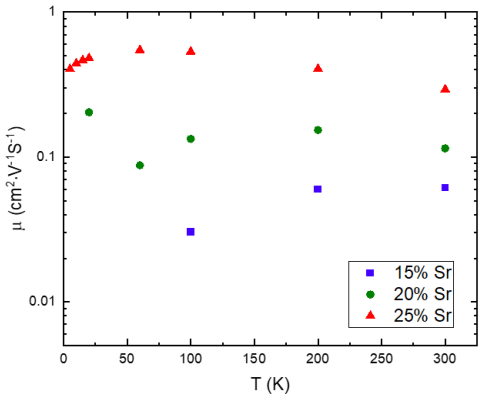

Figure S4. Temperature-dependent mobility for linear Hall response with variation of the magnetic field, assuming $n \approx (R_H e)^{-1}$.

4. Gate measurements at 100K

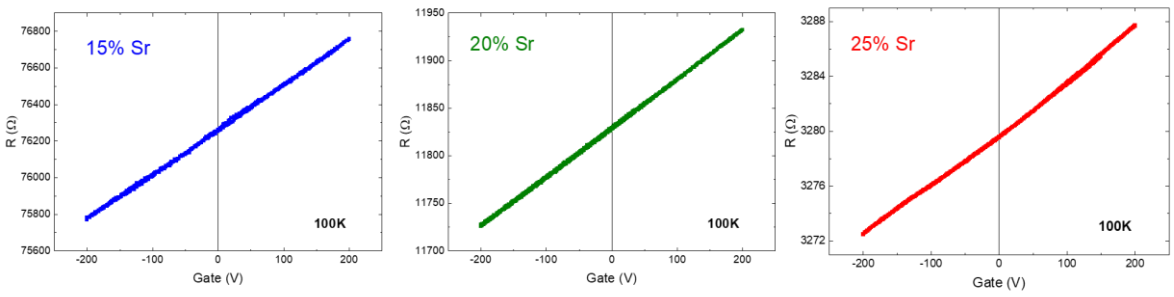

Figure S5. Resistance as a function of the gate voltage for the different $La_{1-x}Sr_xVO_3$ devices measured at 100 K via Hall bar devices.

5. Hall measurements

Hall measurements at various temperatures were conducted for all LSVO devices (Figure S5) in order to estimate the carrier density. For the 25% Sr concentration device, we report a linear Hall response with respect to the magnetic field for all temperatures measured, and only a small

decrease in carrier concentration with cooling, which can be attributed to the LSVO paramagnetic metal phase.[1] Nevertheless, for the 20% Sr concentration device, we report a monotonically decline of the carrier density by an order of magnitude (or more) when cooling, which can be attributed to the LSVO antiferromagnetic metal phase.[1] In addition, for the 20% Sr concentration device, we observed a non-linear Hall response at low temperatures (< 20K). We attempted to fit a two-band model for the non-linear measurements, assuming a negligible 2-dimensional electron gas (2DEG) at the LSVO/STO interface. In this model, the electric conduction (σ) would be composed of a 3-dimensional (3D) contribution from the LSVO film and a 2D contribution from the 2DEG. The model used is based on the following:[2,3]

$$\sigma_{2D} = \begin{pmatrix} D_1 & -A_1 \\ A_1 & D_1 \end{pmatrix} \quad (1)$$

$$D_1 = (n_1\mu_1 q)/[1 + (\mu_1 B)^2] \quad (2)$$

$$A_1 = D_1\mu_1 B \quad (3)$$

Where n and μ are the carrier density and mobility of the conduction channel, B is the external magnetic field, and q is the electron charge. Treating the 3D channel as three paths in parallel through the conduction band minimum (Γ, L and X) gives:

$$\sigma_i = \begin{pmatrix} D_i & -A_i \\ A_i & D_i \end{pmatrix}; i = \Gamma, L, X \quad (4)$$

$$D_i = (n_i\mu_i qt)/[1 + (\mu_i B)^2] \quad (5)$$

$$A_i = D_i\mu_i B \quad (6)$$

And, by assuming an isotropic 3D conduction (Γ = L = X):

$$\sigma_{3D} = \sigma_\Gamma + \sigma_L + \sigma_X = 3\sigma \quad (7)$$

$$\sigma_{tot} = \sigma_{3D} + \sigma_{2D} \quad (8)$$

The results of the two-band model are summarized in Table 1. As can be seen, the fit to the model yielded unphysically low carrier density for the second conduction band (2DEG), suggesting that this model might be inadequate for our case. Another explanation for the non-linear Hall response may be the anomalous Hall effect, typically observed in ferromagnets but also possible in some antiferromagnets.[4] Recent theoretical work suggests that vanadates are candidates for anomalous Hall antiferromagnets due to their orbital ordering,[5,6] which links the two magnetic sublattices by rotation instead of translation, resulting in spin-split electronic bands. While this is not the focus of this work, it will be interesting to see whether future works could link the non-linear Hall effect we observe here with a magnetic origin. For the sake of clarity and focus, regions with more than single-channel conductivity were not included in the main text.

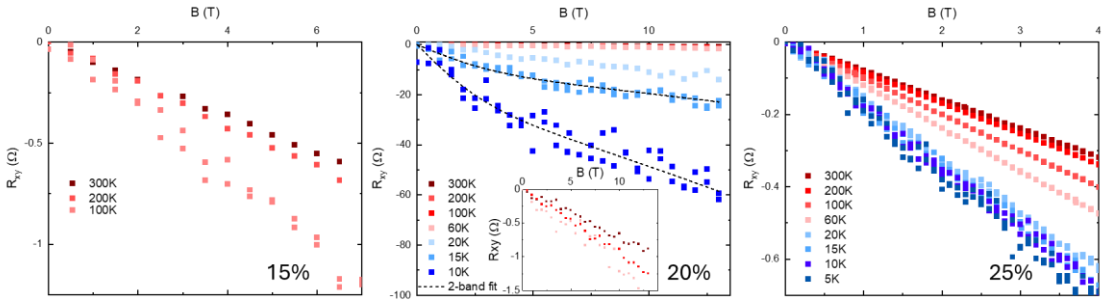

Figure S6. Hall measurements of the LSVO devices at different temperatures. To remove geometric errors, we measured the Hall voltage with both positive and negative fields and then subtracted one from the other: $R_{xy} = (R^{B+} - R^{B-})/2$.[7] When the Hall response is non-linear with respect to the magnetic field for the 20% Sr concentration device, a 2-band fit is presented based on equations 1-8 and the values in Table 1. At 50K and below, we were not able to acquire reliable data for the 15% Sr concentration device.

Table S1. Carrier density (n) and mobility (μ) for fitting the non-linear Hall behavior of the 20% Sr concentration device at low temperatures. n_1 and μ_1 represent a possible 2D conduction at the LSVO/STO interface, and n_2 and μ_2 represent the 3D conduction of the LSVO channel.

T (K)	n_1 (10^6 cm^{-3})	n_2 (10^{20} cm^{-3})	μ_1 ($cm^2V^{-1}S^{-1}$)	μ_2 ($cm^2V^{-1}S^{-1}$)
15K	7.1	3.7	1797	0.17
10K	3.9	1.3	2072	0.27

6. Ruling Out Contribution of Oxygen Vacancies in the Results

The use of STO substrates is necessary here for back gating, leveraging STO's high dielectric constant. However, STO being prone to oxygen vacancies requires special attention to this aspect. We are able to rule out any significant contribution of oxygen vacancies to the transport data presented in the paper, based on multiple considerations, as discussed below.

First and foremost, the key result in this work is that increasing the number of electrons (via the gate), results in a higher resistivity (Figure 3). This signature Mott behavior cannot be explained by extra carriers in STO, particularly considering the small charge modulation. Therefore, the presence of vacancy-induced electrons in the STO would have *countered* the observed effect of the gate's field.

The following points elaborate more on the absence of a significant amount of oxygen vacancies. Their essence is: (1) there is no conductivity between separate devices on one chip. (2) The actual PO_2 on the substrate surface is much higher than the pressure reading. (3) Negligible gate hysteresis is observable.

(1) Our test chips consist of 9 Hall bar devices (see Figure S7). The full microfabrication details can be found in Ref. 41. The process includes etching of the LSVO layer to form the active areas of each device. For each chip, we measured the conductivity between metal contacts on neighboring devices, and the resistance higher than our measurement limit. This proves in a straightforward manner that there is no conductivity arising from the STO substrate.

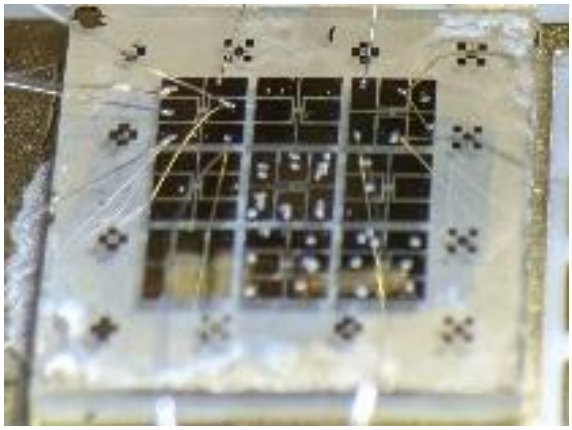

Figure S7. An optical image of the entire 5×5 mm^2 STO chip with 9 Hall bar devices. The grayish/silvery area seen throught the substrate is the metal gate deposited on its backside.

It can further be seen that the substrate (Figure S7) is quite transparent, providing further indication of negligible presence of oxygen vacancies (reduced STO is grayish and it becomes more opaque with increased degree of reduction until becoming black).

(2) While the growth conditions seem somewhat reducing (1000°C, 5×10^{-7} Torr O_2), a closer examination of the growth chamber reveals that the substrate experiences a local environment much richer in oxygen, as illustrated in Figure S8.

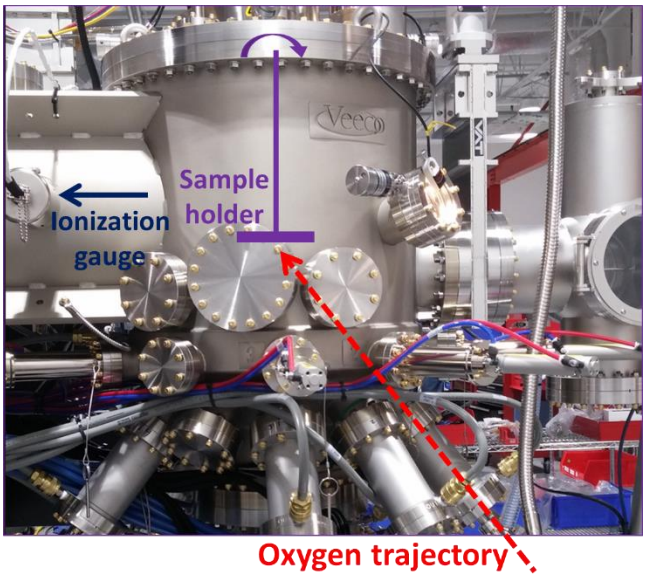

Figure S8. Front view picture of the oxide MBE chamber used for the sample fabrication in this work, with superimposed positions of the ionization gauge, sample holder, and oxygen trajectory. The trajectory is schematic because the actual port where the oxygen is injected is in the backside of the system, but its geometry with respect to the substrate is identical.

The nozzle of the oxygen source is pointing directly at the substrate (Figure S8), while the vacuum gauge is (a) some distance away, and in a receded flange (normal to the image plane), (b) not in line of sight, and (c) closer to the main chamber vacuum pump than it is to the oxygen nozzle. These considerations mean that the substrate exhibits a much high oxygen environment during growth, which we repeatedly find to circumvent conductivity in STO substrates.

(3) In addition, oxygen defects can move readily under electric field, and significant amounts are expected to result in hysteretic behavior when gating[8–10] (Figure 3b). However, all the curves in Figure 3a are showing bi-directional scans, exhibiting no hysteresis, further supporting the absence of significant oxygen vacancies in STO.

7. Gate measurements at low temperatures

Gate measurements were conducted for all LSVO devices at low temperatures (Figure S6). As explained in the main text, we chose to focus on the 100 K measurements because at that temperature, the Hall response to the variation of the magnetic field is linear, and the LSVO is not expected to be close to any structural or magnetic phase transition.[1]

When reviewing the gate results in Figure S5, one must consider three different contributions to the behavior and magnitude of the resistance response to the gate voltage:

1. The dielectric constant of the gate insulator (STO) is considerably higher at low temperatures, which significantly increases the charge induced by the gate. In addition, at low temperatures (< 65K) the STO dielectric constant is affected by the applied electric field following the relation $\varepsilon_{STO} = \frac{1}{A+B \cdot E}$, where A and B are constants for a given temperature.[11]
2. For the 20 and 15% Sr concentration devices, there is a large decrease in carrier density with temperature.
3. The intrinsic correlated-electron behavior as discussed in the main text.

Since the three contributions are interrelated, it is difficult to distinguish their individual contributions.

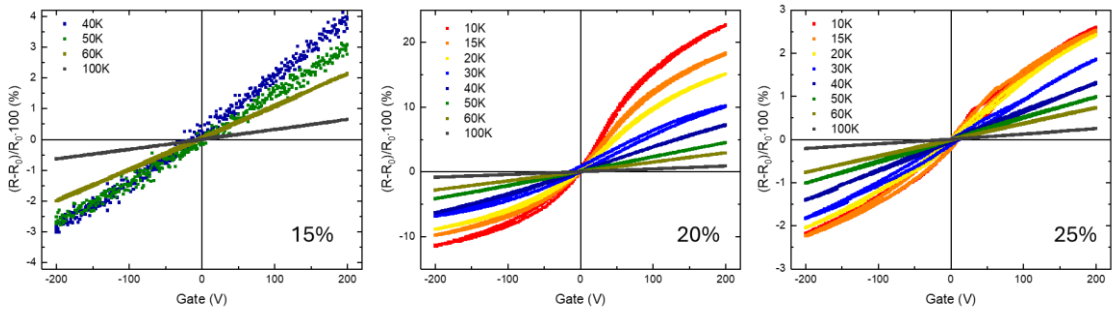

Figure S9. Resistance variation as a function of the gate voltage at different temperatures for different LSVO devices. R_0 is the device resistance under zero bias. The 15% Sr concentration device was too insulating to measure below 40 K.

References

[1] S. Miyasaka, T. Okuda, and Y. Tokura, Phys. Rev. Lett. **85**, 5388 (2000).
[2] C.M. Hurd, S.P. McAlister, W.R. McKinnon, B.R. Stewart, D.J. Day, P. Mandeville, and A.J. Springthorpe, J. Appl. Phys. **63**, 4706 (1988).
[3] M.J. Kane, N. Apsley, D.A. Anderson, L.L. Taylor, and T. Kerr, J. Phys. C Solid State Phys. **18**, 5629 (1985).
[4] L. Šmejkal, A.H. MacDonald, J. Sinova, S. Nakatsuji, and T. Jungwirth, Nat. Rev. Mater. **7**, 482 (2022).
[5] V. Leeb, A. Mook, L. Šmejkal, and J. Knolle, Phys. Rev. Lett. **132**, 236701 (2024).
[6] G. Cuono, R.M. Sattigeri, J. Skolimowski, and C. Autieri, J. Magn. Magn. Mater. **586**, 171163 (2023).
[7] J. Lindemuth, *Hall Effect Measurement Handbook: A Fundamental Tool for Semiconductor Material Characterization* (Lake Shore Cryotronics, Westerville, 2020).
[8] D. Miron, D. Cohen-Azarzar, B. Hoffer, M. Baskin, S. Kvatinsky, E. Yalon, and L. Kornblum, Appl. Phys. Lett. **116**, 223503 (2020).
[9] R. Dittmann, R. Muenstermann, I. Krug, D. Park, T. Menke, J. Mayer, A. Besmehn, F. Kronast, C.M. Schneider, and R. Waser, in *Proc. IEEE* (2012), pp. 1979–1990.
[10] K. Szot, R. Dittmann, W. Speier, and R. Waser, Phys. Status Solidi - Rapid Res. Lett. **1**, R86 (2007).
[11] R.C. Neville, B. Hoeneisen, and C.A. Mead, J. Appl. Phys. **43**, 2124 (1972).